Electronic Supplementary Material (ESI) for Materials Horizons.

Supporting Information

Photocatalytic effect of ZnO on the stability of nonfullerene acceptors and its mitigation by SnO_2 for nonfullerene organic solar cells

*Youyu Jiang, Lulu Sun, Fangyuan Jiang, Cong Xie, Lu Hu, Xinyun Dong, Fei Qin, Tiefeng Liu, Lin Hu, Xueshi Jiang, and Yinhua Zhou**

Wuhan National Laboratory for Optoelectronics, and School of Optical and Electronic Information, Huazhong University of Science and Technology, Wuhan 430074, China

*Corresponding author. E-mail: yh_zhou@hust.edu.cn

Experimental Procedures

1. Materials

The polymer donor material PM6 (PBDB-T-2F) and the non-fullerene acceptor material IT-4F were purchased from Solarmer Materials Inc. The SnO_2 nanocrystal dispersion was obtained from Sigma-Aldrich (Tin(IV) oxide nanoparticle ink, 2.5 wt% in the mixture of butanols, viscosity 4 cP; Product number: 901071). Chlorobenzene, 1,8-diiodooctane (DIO), zinc acetate dihydrate, monoethanolamine, methoxyethanol, and other chemicals were purchased from Alfa Aesar and used without further purification.

2. Device fabrication of NF OSCs

NF OSCs were fabricated with an inverted configuration of ITO/ETL/PM6:IT-4F/MoO_3/Ag. ITO-coated glass was sequentially cleaned with deionized water, acetone and isopropyl alcohol, followed by the 5 min plasma treatment. The ZnO sol-gel precursor solutions were spin-coated onto the ITO substrates at 4000 rpm for 30 s in air, then annealed on a hot plate at 180 °C for 10 min in air. The ZnO precursor solutions were prepared by adding 0.3 g zinc acetate dihydrate and 0.084 g monoethanolamine in 3 mL methoxyethanol, and subsequently stirred for 3 h at room temperature in air. For SnO_2 ETL, the as-purchased SnO_2 dispersion was diluted to 0.2 wt.%, 0.4 wt.%, 1.0 wt.%, respectively, by adding different amount of isopropanol (IPA) in air. The diluted dispersions were spin-coated onto the substrates at 3000 rpm for 30 s in air, and then baked on a hot plate in air for 30 min at different temperature of 100°C, 150°C and 180°C, respectively. The thicknesses of SnO_2 ETL was ca. 5 nm, 10 nm, and 15 nm, for the solution with concentration of 0.2 wt.%, 0.4 wt.%,

1.0 wt.%, respectively. Then, PM6:IT-4F (10 mg: 10 mg) in 1 mL chlorobenzene with 0.5 vol.% 1,8-diiodooctane (DIO) was spin-coated onto the ETL at 1500 rpm for 60 s in a nitrogen (N_2)-filled glove box, followed by a thermal annealing at 100 ^oC for 10 min in the glove box. Finally, MoO_3 (7 nm) and Ag (100 nm) were evaporated on top of the active layers through a shadow mask under a base vacuum of 1×10^{-7} Torr using a thermal evaporator (Mini-Spectros, Kurt J. Lesker). The device area was 0.041 cm^2.

For NF OSCs with slot-die coated SnO_2, diluted SnO_2 (0.04 wt.%) solution was deposited on the ITO substrates at 50 ^oC by slot-die coating and then annealed at 150 ^oC for 30 min in air. Afterward, a solution of PM6:IT-4F blend (10 mg: 10 mg in 1 mL chlorobenzene with 0.5 vol.% DIO) was subsequently doctor-bladed on the SnO_2 layer to form 100 nm-thick blend films in the air. The doctor-blading substrate temperature was 60 °C, and gap height was 60 μm with a 80 mm/s blading speed. The as-prepared devices were further annealed at 100 ^oC for 10 min in N_2-filled glovebox. Finally, MoO_3 and Ag were deposited through a shadow mask with area of 0.041 cm^2 and 1.0 × 1.0 cm^2, respectively.

3. Characterization

Morphology and crystal measurements: TEM images of the SnO_2 nanocrystals were taken on a 300 kV Titan Probe corrected high-resolution transmission electron microscope (HRTEM) (Titan G2 60-300). XRD measurements of SnO_2 films were performed on quartz glass to avoid unnecessary diffraction peaks using a Philips diffractometer (X'pert PRO MRD) using Cu Kα radiation (λ = 1.540598 Å) as the X-ray source. AFM images of films were taken through tapping mode on Shimadzu SPM9700 at ambient conditions.

Optical characterization: Absorption and transmission spectra of films were performed by UV-vis-NIR spectrophotometer (UV-3600, Shimadzu).

MS and FT-IR characterization: The LC-MSD analysis was performed on an Agilent 1100 LC-MS Trap XCT System (Agilent Technologies, USA) using an APCI in the negative ion mode. Fourier transform infrared (FT-IR) spectra of films were collected on a Bruker VERTEX 70.

Work function: Work function of ZnO and SnO_2 films were measured using scanning Kelvin probe. Highly oriented pyrolytic graphite (HOPG) with a work function of 4.5 eV is used as a reference sample.

Photovoltaic performance measurements: *J-V* curves of the NF OSCs were tested under AM 1.5 G irradiation (100 mW/cm2) from a 450 W solar simulator (Newport 94023A-U) in a nitrogen-filled glove box and recorded using a Keithley 2400 source-measure unit. The illumination intensity is calibrated by a standard silicon solar cell. The external quantum efficiency (EQE) test was performed by a EQE system equipped with a standard Si diode using a 150 W xenon lamp fitted with a monochromator (Cornerstone 74004) as a monochromatic light source.

Charge generation and collection characterization: To study the charge generation and collection behaviors, the plots of the J_{ph} versus the effective voltage (V_{eff}) of devices with ZnO and SnO_2 respectively, were measured. The J_{ph} is determined by subtracting the dark current density (J_{dark}) from illumination current (J_{light}), V_{eff} is calculated by subtracting the applied voltage (V_{appl}) from the built-in voltage (V_{bi}). V_{bi} is the voltage when the J_{ph} equals zero.

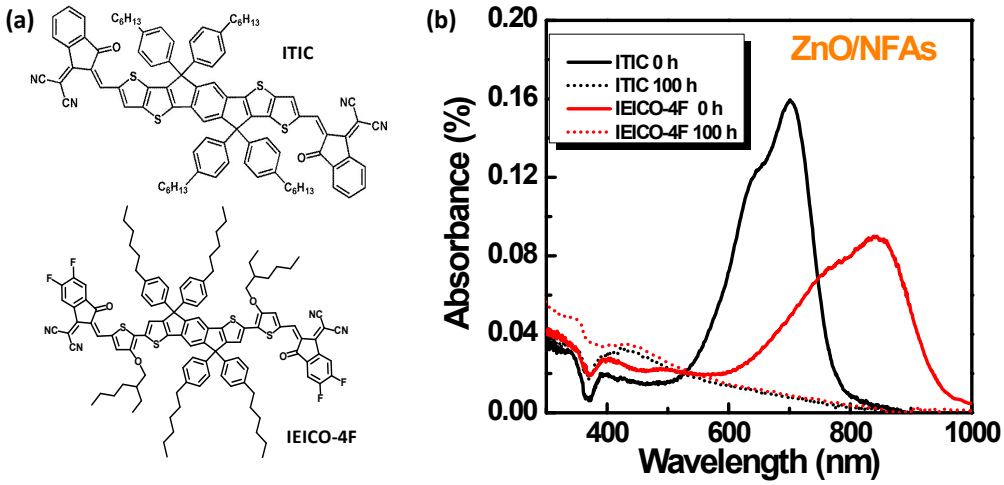

Figure S1. Photocatalytic effect of ZnO on other nonfullerene acceptors. (a) Chemical structure of ITIC and IEICO-4F; (b) UV-vis absorption spectra of ZnO/ITIC and ZnO/IEICO-4F thin films before and after upon continuous AM1.5 illumination.

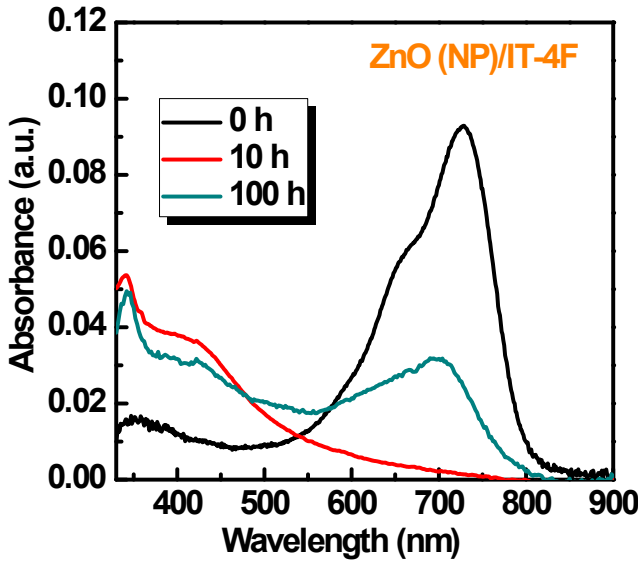

Figure S2. UV-vis absorption spectra of IT-4F thin film on ZnO nanoparticle (NP) ETL upon continuous AM1.5 illumination.

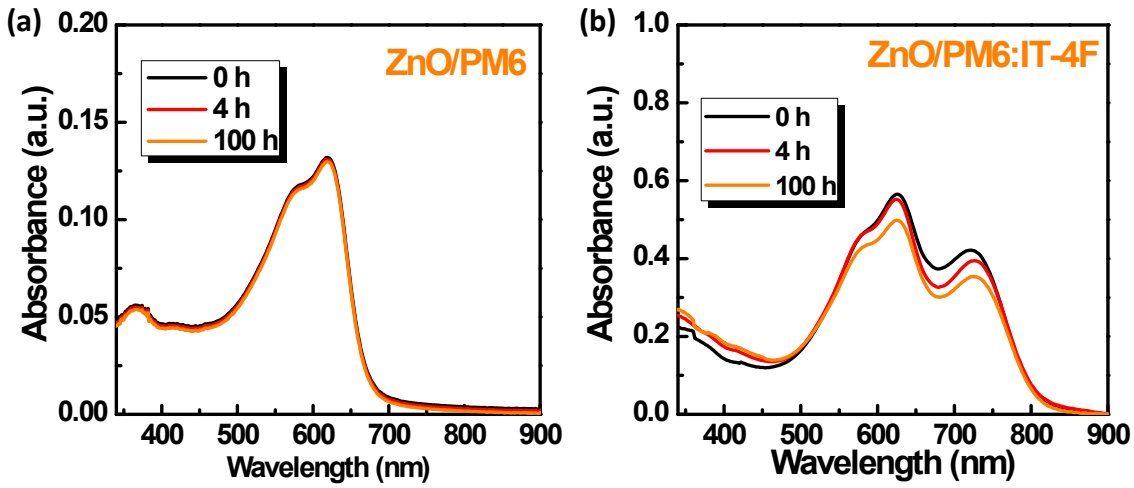

Figure S3. UV-vis absorption spectra of (a) ZnO/PM6 and (b) ZnO/PM6:IT-4F thin films before and after upon continuous AM1.5 illumination.

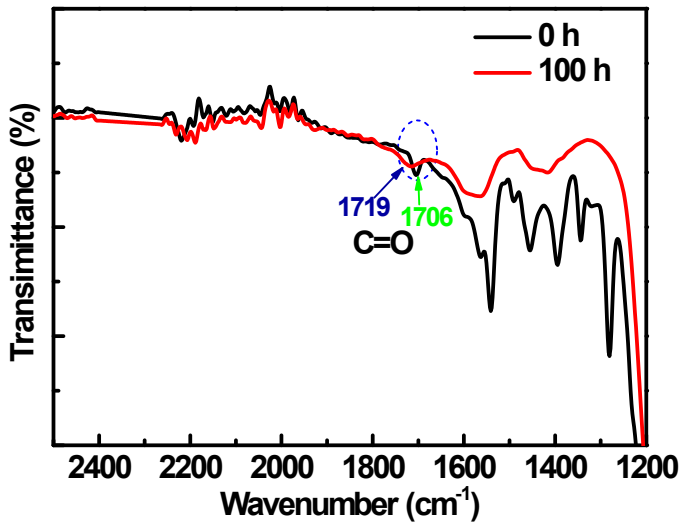

Figure S4. FT-IR spectra of pristine and photodegraded IT-4F films.

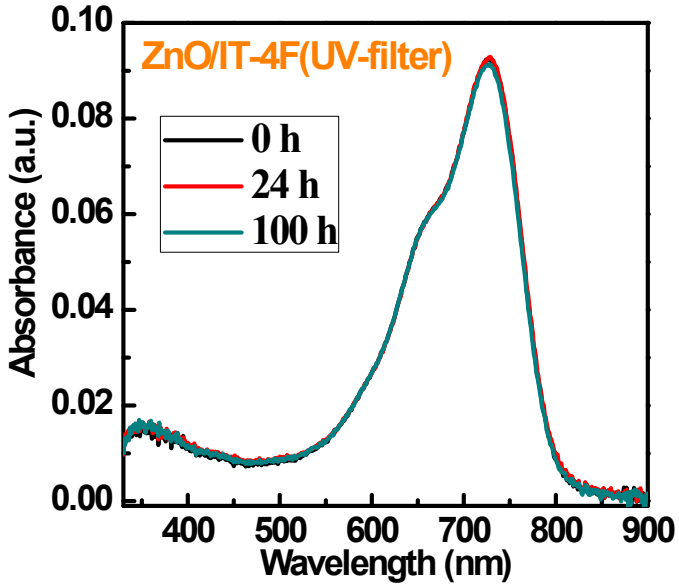

Figure S5. UV-vis absorption spectra of ZnO/IT-4F film upon continuous illumination using a 500-nm cutoff filter.

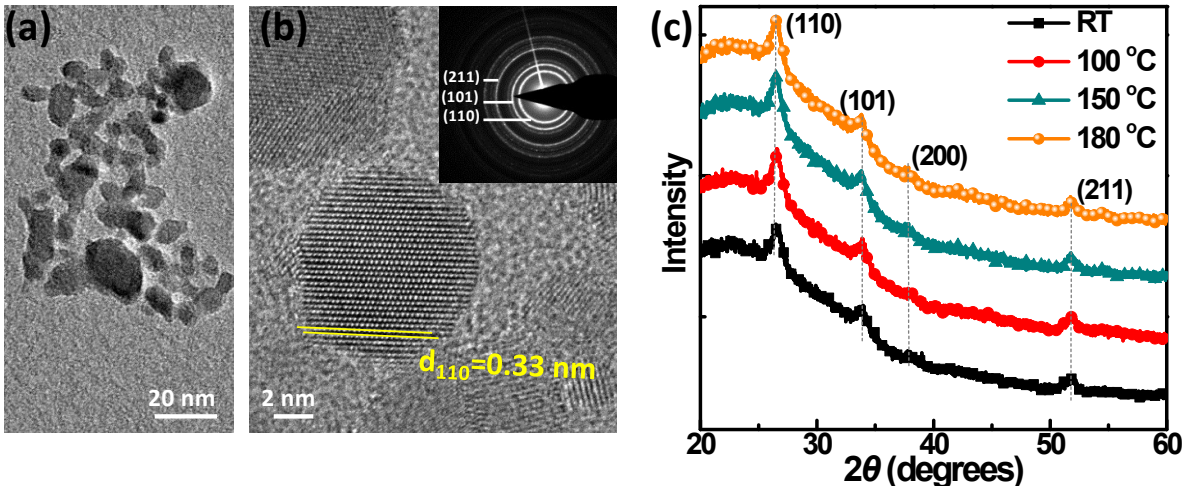

Figure S6. (a) Transmission electron microscopy (TEM) image of SnO_2 nanocrystals. (b) High-resolution TEM (HRTEM) image of SnO_2. Inset shows the selected area electron diffraction patterns. (c) XRD patterns of SnO_2 films grown on quartz glass and annealed at different temperatures.

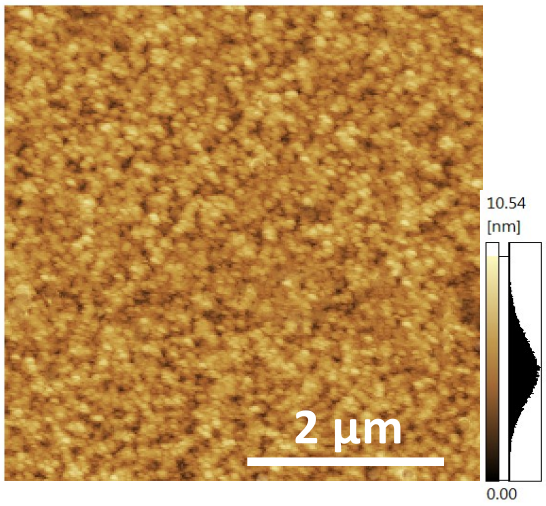

Figure S7. AFM height images of the as-fabricated SnO_2 films deposited on glass substrate.

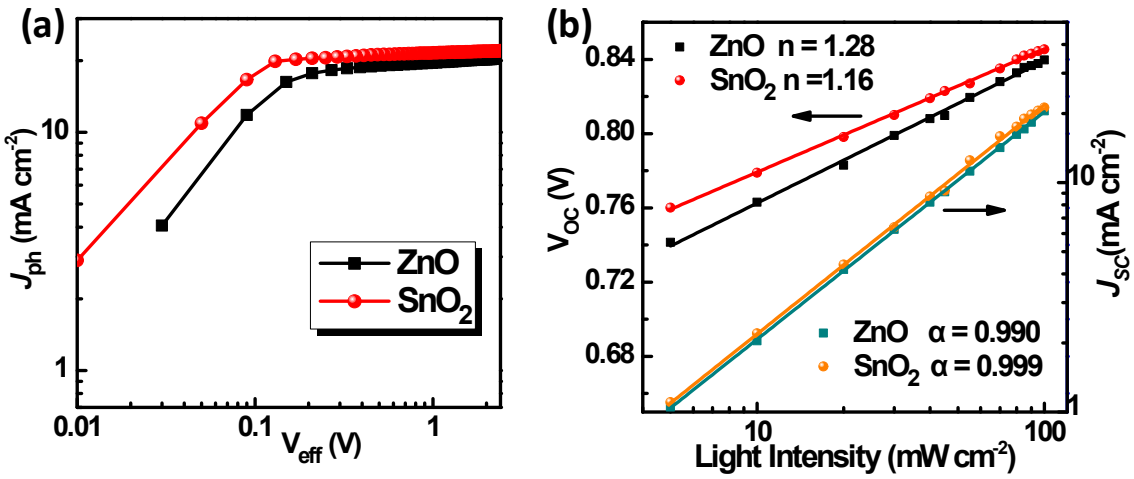

Figure S8. (a) Photocurrent density (J_{ph}) as a function of the effective voltage (V_{eff}) of the NF OSCs with ZnO and SnO_2 ETLs; (b) V_{OC}-P_{light} and J_{SC}-P_{light} characteristics of the NF OSCs with ZnO and SnO_2 ETLs.

To study the charge generation and collection behaviors, the plots of the J_{ph} versus the effective voltage (V_{eff}) of devices with ZnO and SnO_2 respectively, were measured. The J_{ph} is determined by subtracting the dark current density (J_{dark}) from illumination current (J_{light}), V_{eff} is calculated by subtracting the applied voltage (V_{appl}) from the built-in voltage (V_{bi}). V_{bi} is the voltage when the J_{ph} equals zero. Figure S8a shows the plots of the photocurrent density (J_{ph}) versus the effective voltage (V_{eff}). The J_{ph} of both SnO_2 and ZnO based NF-OSCs reach a saturation state ($J_{ph,sat}$) at a V_{eff} of 2 V, suggesting all charge carriers are collected at the electrodes due to the sufficiently high electric field. The $J_{ph}/J_{ph,sat}$ of SnO_2 based cells under short-circuit and the maximum power output conditions are calculated to be 97.8% and 92.2%, compared to the 95.7% and 87.3% of the ZnO based cells, indicating efficient charge dissociation and charge collection of the cells with SnO_2 ETL. The relationship between the *J-V* characteristics and light intensity (P_{light}) are measured to investigate the carrier

recombination. The V_{OC} dependence on P_{light} ($V_{oc} \propto \ln(P_{light})$) of both devices is shown in Figure S8b. Fitting the curves yields slopes of 1.28 kT/q and 1.16 kT/q (where k is Boltzmann constant, T is the kelvin temperature, and q is the elementary charge) for ZnO and SnO_2 based NF OSCs, respectively. The smaller slope of the SnO_2 cell implies reduced Shockley-Read-Hall (SRH) or trap-assisted recombination. The J_{SC} as a function of P_{light} was fitted to the power-law formula of $J_{SC} \propto P_{light}^{\alpha}$. The SnO_2 cell showed a larger exponent α of 0.999 than 0.990 for ZnO cell. The closer the α approaches 1, the less is the bimolecular recombination. Suppression of charge recombination would benifit reduction of energy loss. Therefore, the decreased recombination loss and improved charge collection contribute to the improved performanc*e* in the SnO_2 based NF OSCs.

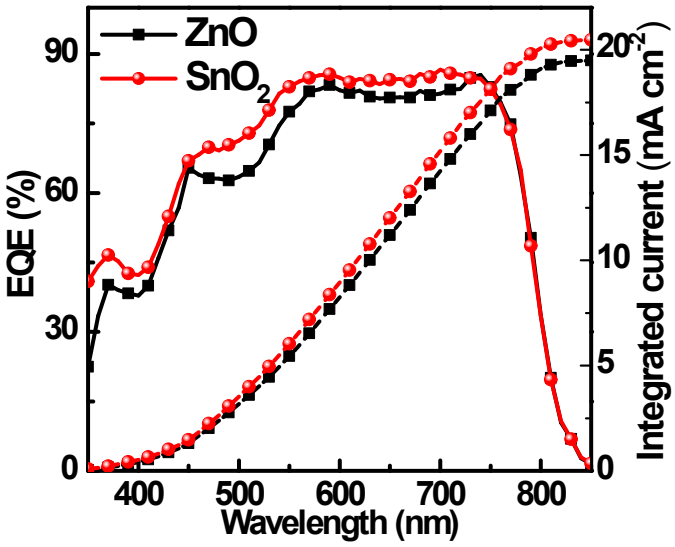

Figure S9. EQE spectra of NF OSCs with ZnO and SnO_2 ETLs, respectively.

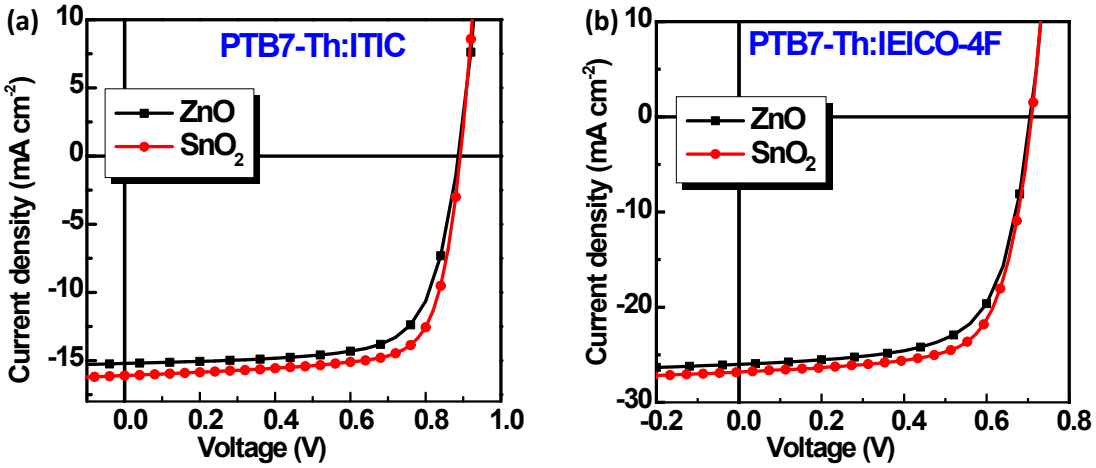

Figure S10. Photovoltaic performance of other nonfullerene active layers of (a) PTB7-Th:ITIC and (b) PTB7-Th:IEICO-4F with ZnO and SnO_2, respectively.

Table S1. Photovoltaic parameters of of other nonfullerene active layers employing ZnO and SnO_2 ETL over 50 devices for each geometry.

Device with active layer	V_{OC} (V)	J_{SC} (mA cm^{-2})	FF	PCE (%)
ZnO/PTB7-Th:ITIC	0.88 ± 0.01 0.89	15.0 ± 0.2 15.2	0.70 ± 0.02 0.71	9.3 ± 0.3 9.6
SnO_2/PTB7-Th:ITIC	0.89 ± 0.01 0.85	15.7 ± 0.2 16.9	0.72 ± 0.02 0.73	10.0 ± 0.2 10.5
ZnO/PTB7-Th:IEICO-4	0.69 ± 0.01 0.70	26.0 ± 0.2 26.0	0.65 ± 0.03 0.66	11.7 ± 0.1 12.0
SnO_2/PTB7-Th:IEICO-4F	0.70 ± 0.01 0.71	26.6 ± 0.2 26.8	0.68 ± 0.02 0.69	12.6 ± 0.1 13.1

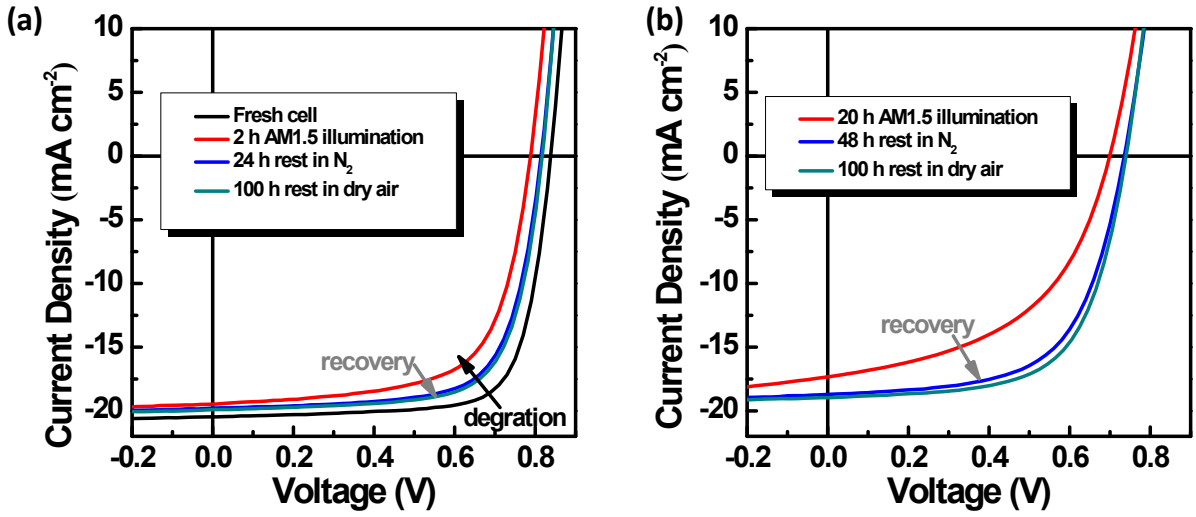

Figure S11. Performance degradation and recovery test of a PM6:IT-4F cell with ZnO ETL. (a) *J-V* characteristics of the NF cell after 2 h AM1.5 illumination in N_2, followed by storage in N_2 for 24 h and, additionally, dry air for 100 h; (b) the cell was then illuminated in N_2 for total 20 h. *J-V* characteristics of the cell after total 20-h illumination, followed by storage in N_2 for 48 h and, additionally, dry air for 100 h.

Table S2 The photovoltaic characteristics of PM6:IT-4F photodegraded cells employing ZnO ETL after AM1.5 illumination in N_2 upon storage in N_2 and dry air for several hours.

ZnO ETL	V_{OC} (V)	J_{SC} (mA cm^{-2})	FF	PCE (%)
Fresh cell	0.83	20.5	0.75	12.8
2 h AM1.5 illumination	0.79	19.5	0.65	10.1
24 h rest in N_2	0.82	19.7	0.69	11.2
100 h rest in dry air	0.82	19.9	0.71	11.6
20 h AM1.5 illumination	0.69	17.4	0.50	6.0
48 h rest in N_2	0.73	18.7	0.61	8.3
100 h rest in dry air	0.74	18.9	0.63	8.9

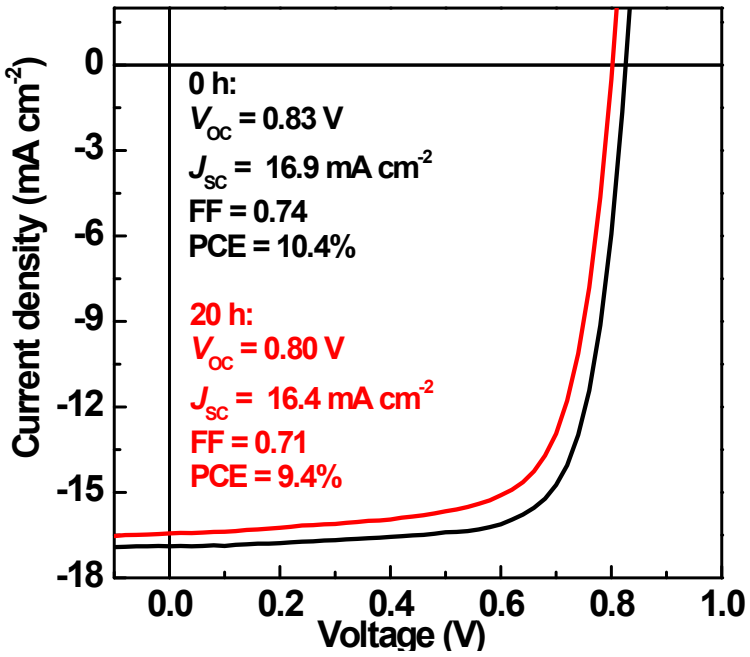

Figure S12. *J-V* characteristics of the PM6:IT-4F cells with ZnO ETL before and after illumination when using a 500-nm cutoff filter.

Table S3. Photovoltaic parameters of PM6:IT-4F NF OSCs employing SnO_2 ETL annealed at various temperature.

SnO_2 ETL	V_{OC} (V)	J_{SC} (mA cm^{-2})	FF	PCE (%)
RT	0.83 ± 0.01 0.84	20.2 ± 0.3 20.3	0.71 ± 0.02 0.72	11.9 ± 0.2 12.1
100 °C	0.85 ± 0.01 0.85	21.2 ± 0.2 21.3	0.77 ± 0.02 0.77	13.7 ± 0.2 13.9
150 °C	0.85 ± 0.01 0.85	21.3 ± 0.2 21.3	0.77 ± 0.01 0.78	13.8 ± 0.2 14.1
180 °C	0.83 ± 0.01 0.83	21.20 ± 0.18 21.6	0.75 ± 0.01 0.75	13.2 ± 0.2 13.5

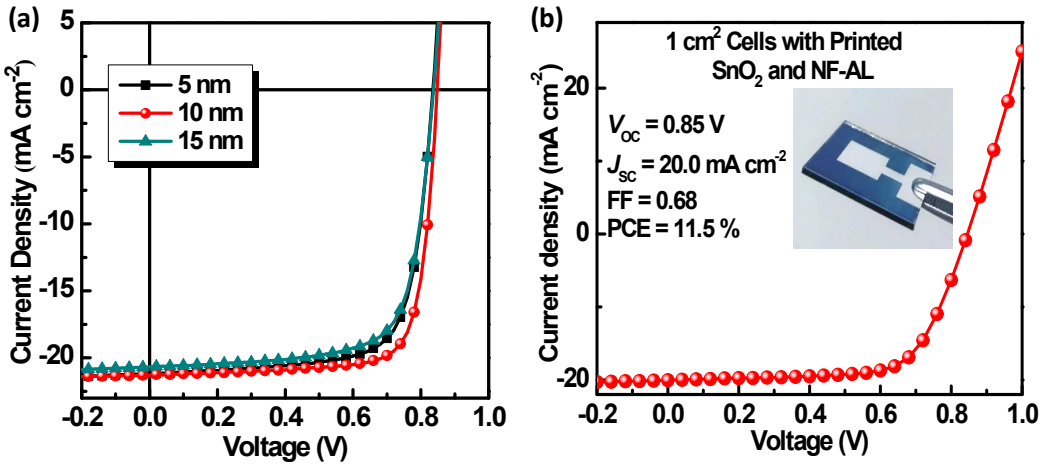

Figure S13. (a) *J-V* characteristics of the PM6:IT-4F OSCs using SnO_2 with different thicknesses; (b) *J-V* curves of 1 cm^2 NF OSCs with slot-die printed SnO_2 ETL and doctor-bladed PM6:IT-4F nonfullerene active layer.